PAPER • OPEN ACCESS

Towards pair production in the non-perturbative regime

To cite this article: F C Salgado *et al* 2021 *New J. Phys.* **23** 105002

View the article online for updates and enhancements.

New Journal of Physics

The open access journal at the forefront of physics

PAPER

CrossMark

Towards pair production in the non-perturbative regime

F C Salgado[1,2,*] , K Grafenstein[3,4], A Golub[5], A Döpp[3,4], A Eckey[5], D Hollatz[1,2],
C Müller[5], A Seidel[1,2], D Seipt[1,2] , S Karsch[3,4] and M Zepf[1,2]

1 Institut für Optik und Quantenelektronik, Friedrich-Schiller-Universität Jena, Max-Wien-Platz 1, 07743 Jena, Germany
2 Helmholtz-Institut Jena, Fröbelstieg 3, 07743 Jena, Germany
3 Centre for Advanced Laser Applications, Ludwig-Maximilians-Universität München, Am Coulombwall 1, 85748 Garching, Germany
4 Max-Planck-Institut für Quantenoptik, Hans-Kopfermann-Strasse 1, 85748 Garching, Germany
5 Institut für Theoretische Physik I, Heinrich-Heine-Universität Düsseldorf, Universitätsstraße 1, 40225 Düsseldorf, Germany
* Author to whom any correspondence should be addressed.

E-mail: felipe.salgado@uni-jena.de

Abstract

The interaction of light with the quantum-vacuum is predicted to give rise to some of the most fundamental and exotic processes in modern physics, which remain untested in the laboratory to date. Electron–positron pair production from a pure vacuum target, which has yet to be observed experimentally, is possibly the most iconic. The advent of ultra-intense lasers and laser accelerated GeV electron beams provide an ideal platform for the experimental realisation. Collisions of high energy γ-ray photons derived from the GeV electrons and intense laser fields result in detectable pair production rates at field strengths that approach and exceed the Schwinger limit in the centre-of-momentum frame. A detailed experiment has been designed to be implemented at the ATLAS laser at the centre of advanced laser applications. We show full calculations of the expected backgrounds and beam parameters which suggest that single pair events can be reliably generated and detected.

1. Introduction

The creation of matter purely from the interaction of two light quanta in vacuum is one of the most fundamental predictions [1] in modern physics to elude experimental investigation to date. The opportunity afforded by the advent of ultra-intense lasers capable of reaching intensities of 10^{21} W cm^{-2} and beyond [2, 3] and simultaneously driving laser-wakefield accelerators (LWFA) capable of reaching multi-GeV energies [4–6] over cm-distance scales has brought the challenge of testing vacuum pair creation—once thought insurmountable—into reach for mid-scale facilities. First concrete designs and proposals were made for the GEMINI laser system at the Rutherford Laboratory, UK [7] with several groups discussing aspects and possible geometries of such experiments since [8–12].

The creation of matter–antimatter pairs from the quantum vacuum occurs either via the Schwinger [13, 14] or the Breit–Wheeler (BW) mechanism [1] or combinations thereof [15, 16]. The Schwinger mechanism requires a field strong enough and capable to perform the work equivalent to the rest mass energy of the particle to create a particle pair over its reduced Compton wavelength $\mathcal{E}_S = m_e c^2/(e\lambda_c) = 1.3 \times 10^{18}$ V m^{-1} corresponding to a laser intensity of $I \approx 10^{29}$ W cm^{-2}. Pair production through the BW reaction [1] in its simplest form requires the collision of two energetic photons:

$$\gamma + \gamma' \to e^+ + e^-. \tag{1}$$

In the BW process, the energies of the participating photons with $E = \hbar\omega$ must be such that the total collision energy is sufficient to produce the rest mass energy of the electron–positron pair. The physics of the BW pair production process is governed by the two Lorentz and gauge invariant parameters: a_0 and χ_γ. The normalised laser vector potential, which is given in rationalized natural units ($c = \hbar = \epsilon_0 = 1$) by $a_0 = e\mathcal{E}/(m_e\omega_0)$, with the laser electric field amplitude $\mathcal{E}$, serves as the inverse Keldysh parameter of the problem.

The quantum nonlinearity (or quantum efficiency) parameter χ of a (massive) particle is the ratio of the laser field strength in the particle's rest frame to the Schwinger field $\mathcal{E}_S$. For the collision of an electron with an intense field at an angle θ it can be expressed as $\chi_e = (1 - \beta_e \cos\theta)\gamma_e \mathcal{E}/\mathcal{E}_S$. More pertinently, for our considerations for the collision of a γ-ray photon of frequency ω_γ with an intense laser beam at the angle θ the quantum nonlinearity parameter reads

$$\chi_\gamma = a_0 \frac{\omega_\gamma \omega_0 (1 - \cos\theta)}{m_e^2}. \tag{2}$$

In analogy to atomic ionisation phenomena [17], pair creation experiments can be divided into three regimes, distinguished by the values of a_0 and χ_γ:

(a) The linear regime ($a_0 \ll 1$ and $\chi_\gamma \ll 1$), first considered by Breit and Wheeler [1], where a binary collision of two photons with frequencies ω_0, ω_γ provides sufficient energy to produce an electron–positron pair. In the centre-of-momentum (COM) frame [18] the threshold condition can be written as $\omega_0 \omega_\gamma \geqslant m_e^2$. This is analogous to atomic photo-ionisation by a photon exceeding the binding energy of the bound electron.

(b) The multi-photon regime ($a_0 \lesssim 1$, $\chi_\gamma < 1$), where $N \geqslant N_0$ photons from the intense field collectively contribute to meeting the pair-production threshold

$$\gamma + N_{\text{laser}}\,\omega_0 \to e^+ + e^-. \tag{3}$$

The minimum number of photons N_0 required for the reaction to occur is determined by the threshold for the multi-photon channels $(N\omega_0)\omega_\gamma \geqslant m_\star^2$, where $m_\star = m_e\sqrt{1 + a_0^2/2}$ is the intensity-dependent effective mass of the leptons [15, 19]. In the multi-photon regime, the N-photon channels exhibit a perturbative scaling with the Nth power of the laser intensity.

(c) The non-perturbative, quasi-static strong-field regime $a_0 \gg 1$, where typically a very large number of laser photons are required to overcome the threshold. In this regime, the strong laser field can be considered to be 'deforming' the mass-gap between the negative and positive continuum. This is analogous to the suppression of the atomic potentials where strong-field ionization proceeds by either tunnelling of the wavefunction through (or propagation over) the potential barrier. In this regime, the pair production rate depends strongly on the value of the quantum parameter χ_γ. For $\chi_\gamma \ll 1$ the pair production rate scales as $P \sim \chi_\gamma \exp(-8/3\chi_\gamma)$, with an exponential suppression typical for tunnelling processes [18–20]. Contrary, if $\chi_\gamma \gg 1$ the rate scales as $P \sim \chi_\gamma^{2/3}$, which could be considered the equivalent of the over-the-barrier regime.

An experimental investigation of the *linear* regime (a) has been precluded to date by the small cross-section (about 150 mb) and the lack of photon beams with the required energy *and* luminosity. Consequently, the linear BW process is still considered as the most difficult fundamental QED process to be observed experimentally on Earth.

Despite the importance of this reaction in cosmology and its relevance to γ-ray colliders it has yet to be demonstrated experimentally in the absence of charged particles in the interaction region and therefore free of all competing processes. First experimental evidence of the non-linear BW process was obtained in 1996 in an experiment in which pairs were observed in laser-electron beam interactions. In this experiment, performed at SLAC, 47 GeV electron bunches collided with an intense ($I = 5 \times 10^{17}$ W cm^{-2}, $a_0 = 0.4$, $\lambda = 527$ nm) laser pulse [21–23]. The interaction resulted in the production of Compton γ-rays with photon energies up to 29.2 GeV. At this very high γ-energy, conservation of energy demands at least 5 laser photons to take part in the interaction, placing this experiment into the multi-photon regime (b).

Figure 1 shows a plot of the different interaction regimes as a function of γ-ray energy ($E_\gamma = \hbar\omega_\gamma$) and laser strength a_0. The experiment detailed here assumes e-beam parameters of 2.5 GeV electrons and $a_0 \approx 66$, placing it into the unexplored quasi-static regime of strong-field pair production, case (c).

In the following we present the detailed design case developed by the Research Collaboration 'Probing the Quantum Vacuum' [24] for the ATLAS laser facility. We show various aspects of the current design and highlight that single lepton detection above background is possible at experimentally accessible rates in the current configuration. We highlight the trade-off between signal rates and the background which affects the signal-to-noise ratio (SNR) in this experimental configuration, which optimise for relatively thin converter foils and intensities below the theoretical maximum achievable. We also present full shielding simulation with GEANT4 that minimises the production Bethe–Heitler pairs from apertures etc and demonstrate detector simulations showing an SNR of ≈ 10 for our design point.
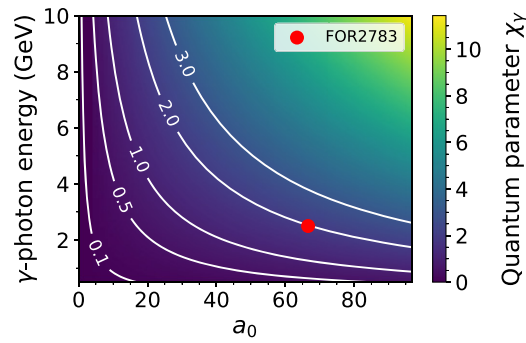
Figure 1. Dependence of χ_γ on γ-ray energy and a_0 for $\lambda = 800$ nm. The FOR2783 experiment design point is shown in red: $E_\gamma = 2.5$ GeV and $a_0 = 66$ ($I = 9.5 \times 10^{21}$ W cm^{-2}).
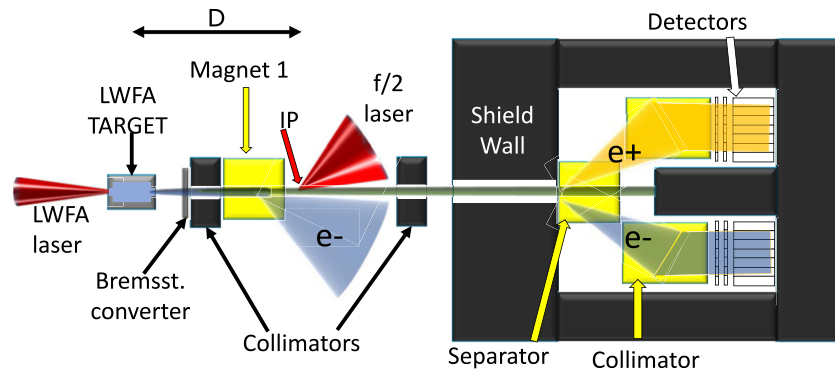

Figure 2. Experimental layout of the FOR2783 experiment at the Centre for Advanced Laser Applications (CALA). Two laser beams are required for the experiment. The 'LWFA-laser' beam is responsible for accelerating monoenergetic electron beams that interact with a converter foil generating bremsstrahlung gamma photons. The electron beam is deflected outside of the main experimental axis while the γ-beam interacts with a second tightly focus (F/2) 'collider' laser beam. The interaction promotes the creation of electron–positron pairs through strong-field interactions. The gamma photons together with the created pairs travel towards the detectors where a beam dump for the high-energy photons is placed and a pair dipole magnet guides the particles towards the single particle detectors.
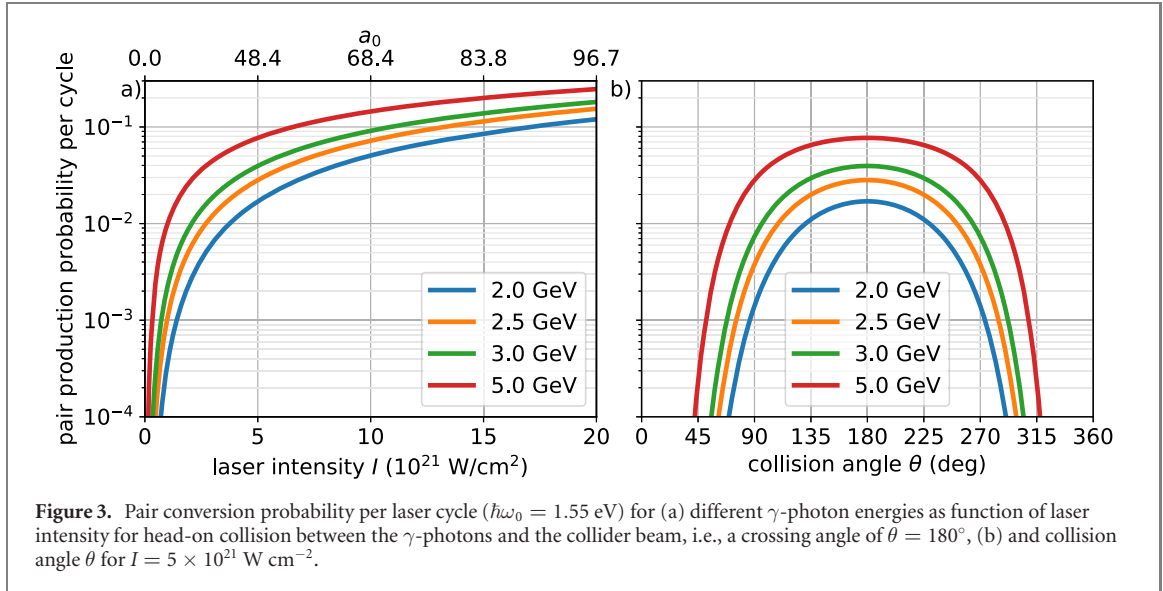
2. Experimental design

The challenge of investigating the BW phenomenon in a laboratory has always been recognised as formidable and engaged physicists for decades. The first proposal to perform an 'all-optical' experiment based on CPA laser technology [7, 25] and LWFA accelerators [5, 26, 27] was centred on the Astra-Gemini laser [7], which demonstrated the key components of the current experimental design—in particular the analyser magnet system [28], LWFA beams with 2.5 GeV energy from [29] and successful timing overlap of an LWFA driving laser and the collider laser beams [30].

The schematic layout of the experiment is as shown in figure 2 and follows the same basic arrangement first introduced in the GEMINI campaign [7, 28]. Two intense, PW-class laser beams are required to drive the experiment, a weakly focussed LWFA beam and the tightly focussed high-intensity beam. In the case of our experiment the ATLAS laser at CALA produces a single beam with the energy limited to 45 J (of the available 60 J) in 30 fs and consequently a power of 1.5 PW with a central wavelength of $\lambda = 800$ nm. This beam is then split spatially into a central part containing 9.5 J for the ultra-intense beam and ring-shaped beam containing about 30 J (after splitting losses) to drive the multi-GeV laser-wakefield accelerator.

The weakly focussed 'LWFA-laser' beam accelerates electrons to multi-GeV energies using the LWFA method [27]. The electrons then interact with a high-Z converter foil to produce high-energy bremsstrahlung γ-ray photons. The electrons are deflected by the first magnet to an electron spectrometer, while the bremsstrahlung γ-rays interact with the tightly focussed 'collider' laser at the interaction point (IP). A key consideration is minimising the distance D from the LWFA stage to the IP to increase the γ-photon flux at the IP. The installation into a multi-purpose facility favours the use of permanent magnets with field strengths of approximately 1 T.

At the IP, the interaction between the γ-photons and the collider laser produces BW pairs that propagate towards the analyser magnet system consisting of a separator and collimator magnet located after a

Figure 3. Pair conversion probability per laser cycle ($\hbar\omega_0 = 1.55$ eV) for (a) different γ-photon energies as function of laser intensity for head-on collision between the γ-photons and the collider beam, i.e., a crossing angle of $\theta = 180°$, (b) and collision angle θ for $I = 5 \times 10^{21}$ W cm^{-2}.

radiation shield wall. This allows the intense γ-ray beam to be separated from the pairs, which are detected on a single event sensitive detector array consisting of Cherenkov calorimeters and a pixelated LYSO array. Calibration of the detector system will be performed by placing a thin foil source of Bethe–Heitler pairs in the IP.

2.1. Pair creation probability and optimal intensity

The primary experimental parameters of laser intensity and γ-ray energy are set by using the available laser energy to achieve high pair creation probability in the IP. We base our experimental design on the previously published theoretical work considering the non-linear BW interaction [19, 31], and note the significant body of further work e.g. [8, 32–41].

Assuming that a γ-ray photon of energy E_γ collides with a linearly polarized laser beam of intensity I_{laser}, photon energy $\hbar\omega_0 = 1.55$ eV, the probability rate of pair creation dP/dt of the nonlinear BW process is given, in rationalized natural units and employing the locally constant field approximation, by [19]

$$\frac{dP}{dt} = -\frac{\alpha m_e^2 \chi_\gamma}{16\omega_\gamma} \int_{z_0}^{\infty} dz \frac{8u+1}{\sqrt{z}\sqrt{u^3(u-1)}} \text{Ai}'(z), \quad (4)$$

with $z_0 = (4/\chi_\gamma)^{2/3}$ and $u = (z/z_0)^{3/2}$. Figure 3(a) shows the pair conversion probability per cycle of the laser pulse, i.e., the rate in (4) integrated over one laser cycle, as a function of the laser intensity. The exponential suppression of the pair production probability predicted by theory for a non-perturbative process below threshold is clearly visible at low intensities. At high intensities (for values of $\chi > 1$) the effective non-linearity q of the pair production probability $P(a_0) \propto I^q$ reduces significantly and the pair production probability per cycle exceeds 10% per incident γ-photon requiring depletion of the γ-photons to be taken into account.

The optimal intensity to maximise the pair yield for fixed laser power is determined by the effective non-linearity parameter q for this experimental configuration. Under the assumption of fixed laser power and a large γ-spot area $A_\gamma > A_{laser}$ the number of γ-photons interacting with the intense field increases linearly with focal spot area as $N_\gamma \propto A_{laser}$, while the intensity decreases linearly with $I \propto A_{laser}^{-1}$.

In the exponentially suppressed regime, characterised by a high effective non-linearity q, it is clearly desirable to maximise the laser intensity. However, in the limit of high intensities where $q < 1$ the pair yield $N_{pairs} \sim N_\gamma P$ increases sub-linearly and larger laser spots at the optimum intensity rather than the highest intensity result in maximum pair yield. The ideal intensity can be seen to be in the range of $0.5 \ldots 3 \times 10^{22}$ W cm^{-2} in figure 4 for the accessible electron-beam energy range of $1 \ldots 5$ GeV. We choose to base our design on an electron beam energy of 2.5 GeV and a peak intensity close to 10^{22} W cm^{-2}, where $q \approx 1$. The collision angle between the γ-ray beam and the laser pulse was chosen to be 162° which does not significantly reduce the pair yield as compared to the theoretical optimum of 180° (see figure 3(b), a detailed explanation for the chosen angle is given in the following section 3.1). The potential gains in pair yield from higher electron beam energies would be offset by the increase in the magnet length and therefore D assuming a constant γ-ray divergence set by the electron beam.
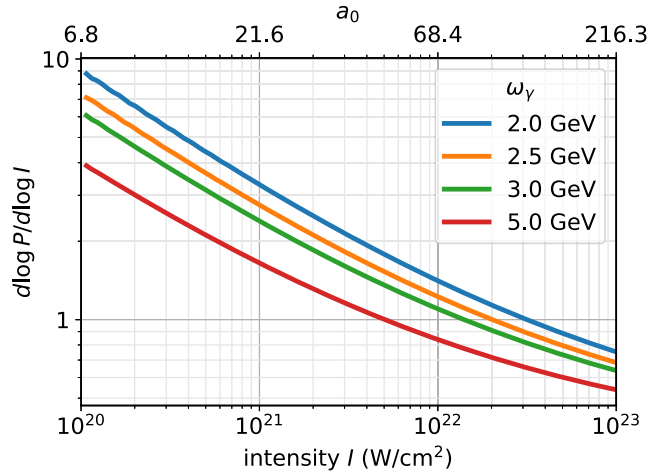
Figure 4. Logarithmic derivative of the pair production yield (slope of the curves in figure 3(a)). The value 1 is the optimal experimental case for a constant density of γ-rays in a spot size much larger than the laser spot size.
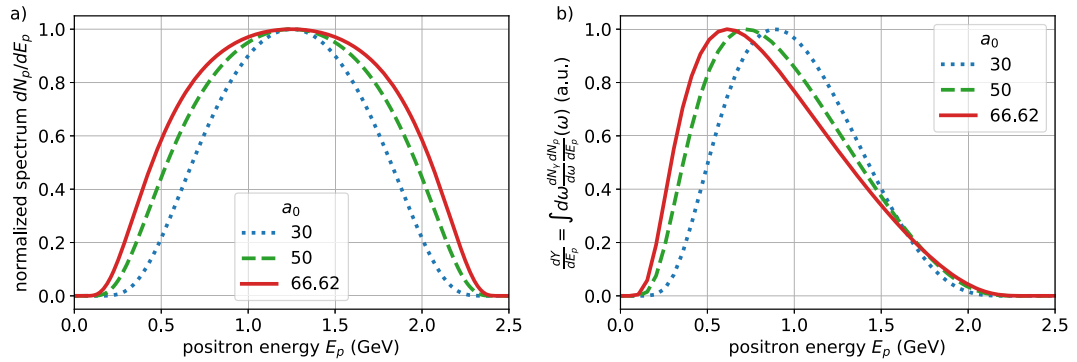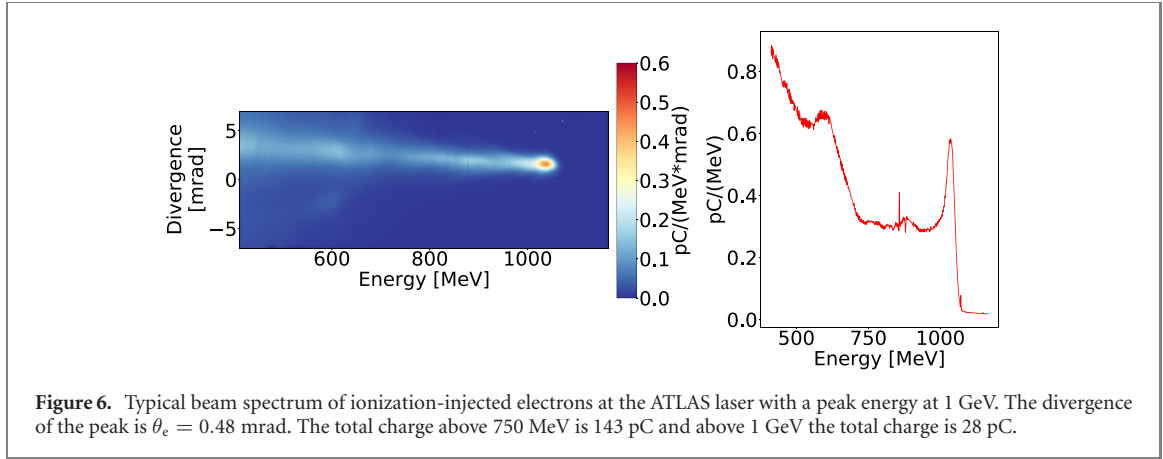

Figure 5. Normalized spectra of produced pairs for (a) a monoenergetic γ-ray with energy of $E_\gamma = 2.5$ GeV, and (b) for the bremsstrahlung spectrum expected from a 50 μm thick converter foil, for different values of the normalized vector potential: $a_0 = 30$, $a_0 = 50$, and $a_0 = 66.62$. A monoenergetic γ-beam produces a pair spectrum centred at $E_\gamma/2$. The experimental spectra are shifted towards lower energies and broadened due to the bremsstrahlung γ-ray spectra.

The expected pair spectrum is then determined by the γ-ray spectrum. For a monoenergetic γ-ray beam, the energy spectra for the pairs are symmetrical and centred at $E_\gamma/2$ as is to be expected from the kinematics. For our parameters, the most efficient approach to generate a γ-beam is via bremsstrahlung in a high-Z foil (details see below) placed shortly after the LWFA target as seen in figure 2, which results in broad spectra with the highest photon numbers produced at low energies. This leads to asymmetrical experimental pair spectra shifted to lower energies. Figure 5 shows the positron energy spectrum broadening and shifting for different values of the normalized vector potential a_0.

2.2. Laser wakefield accelerator and γ-ray beam production

The LWFA stage is designed to be capable of producing multi-GeV electron beams. The LWFA drive beam will contain an energy of up to 30 J, focussed with an $f/40$ parabolic mirror. Experiments with similar laser power have previously been used to generate electron beams of up to 7.8 GeV [42]. Using a conservative estimate the setup is thus expected to allow stable generation of electron beams with an endpoint energy of 2.5 GeV. While these electron beam energies are substantially below the ultimate limit of what is achievable with 30 J in the LWFA beam [4] using external guiding, the simplicity of a self-guided accelerator [29] is preferred for this initial experiment.

First tests with the ATLAS laser were performed at a reduced laser energy of ≈ 5 J, using an $f/30$ focussing geometry and a 20 mm-long slit nozzle with a plateau electron density of $\approx 10^{18}$ cm^{-3}. Electrons were injected via ionization-induced process in a gas mixture containing 96% hydrogen and 4% nitrogen and routinely reached a peak energy of around 1 GeV. A typical electron spectrum with an FWHM divergence in the peak of $\theta_e = 0.48$ mrad can be seen in figure 6. The observed beam energies follow approximately the scalings for matched acceleration in the bubble regime where the maximum energy gain

Figure 6. Typical beam spectrum of ionization-injected electrons at the ATLAS laser with a peak energy at 1 GeV. The divergence of the peak is $\theta_e = 0.48$ mrad. The total charge above 750 MeV is 143 pC and above 1 GeV the total charge is 28 pC.

is given by [43]

$$\Delta E_{\text{max}} \ (\text{GeV}) \approx 1.7 \cdot (P[100 \ \text{TW}])^{1/3} \cdot (n_e[10^{18} \ \text{cm}^{-3}])^{-2/3} \cdot (\lambda[800 \ \text{nm}])^{-4/3}, \tag{5}$$

which evaluates to $\Delta E_{\text{max}} > 2.5$ GeV for a driving laser power of $P_L > 300$ TW at $\lambda = 800$ nm and a plasma density $n_e < 10^{18}$ cm^{-3}. It is therefore expected that operation at the design energy of the experiment (30 J, $P_L \approx 1$PW) and at matching density will lead to the desired peak energies above 2.5 GeV.

The LWFA stage is followed by a thin tape target, to separate the remaining laser light of LWFA beam from the remaining set-up by forming a highly reflective plasma mirror [44], while negligibly perturbing the electron beam.

3. Bremsstrahlung conversion

The conversion of the electron beam to γ-rays takes place in a high-Z tungsten target for high efficiency. Tungsten has among the highest radiation yield of readily available target materials (368 MeV cm^2 g^{-1} for interaction with a 2.5 GeV electron).

Optimising the bremsstrahlung conversion is a critical part of the optimising the signal and controlling the background. As is well known the overall bremsstrahlung yield optimises for target lengths close to the material radiation length, $L_{\text{rad}} = 3.5$ mm in the case of tungsten. The bremsstrahlung photon spectrum produced by a relativistic charged particle with energy E_0 passing through a thin converter target of high-Z material with radiation length equal to L_{rad} and thickness L produces a radiation spectrum given by the approximated equation [45]:

$$\frac{dN_\gamma}{dE_\gamma} = \frac{L}{E_\gamma L_{\text{rad}}} \left[\frac{4}{3} - \frac{4}{3} \frac{E_\gamma}{E_0} + \left(\frac{E_\gamma}{E_0} \right)^2 \right]. \tag{6}$$

In figure 7(a) we see how the Bremsstrahlung spectrum evolves for increasing converter thickness L. The rapid reduction of the pair production probability with decreasing γ energy places the emphasis on optimising the flux of high energy γ-photons with energy $E_\gamma > 0.9E_0$. The softening of the spectrum due to electron energy loss and scattering of the high energy γ-rays shifts the optimum to lengths of $L < L_{\text{rad}}$. Note the negligible increases in yield above $0.9E_0 = 2.25$ GeV as the target thickness is increased from 1.0 mm to 2.5 mm.

Multiple scattering of the electrons with increasing L also increases the FWHM angular distribution of the emitted photons. As shown in figure 7(b), the angular distribution begins to exceed the limit for a collimated beam reducing the gains in flux at the IP, with 90% of the maximum γ-flux at the IP reached $L \approx 0.4L_{\text{rad}}$. Figure 7(c) shows the hard γ-flux for different tungsten converter target thicknesses at the IP. Note that although the overall Bremsstrahlung yield increases the hard γ-flux saturates due to increased divergence and softening of the spectrum with increased converter thickness. The simulated γ-flux distribution for different converter targets is shown in figure 8 with the increasing divergence and stochastic nature of the photon distribution visible.

3.1. Photon–photon interaction point
The IP is positioned as close as possible to the magnet exit to maximise the number of γ-photons interacting with the high-intensity laser field by increasing the γ-photon flux as discussed already in section 2. The bremsstrahlung converter is followed by the electron beam dipole magnet with a deflection
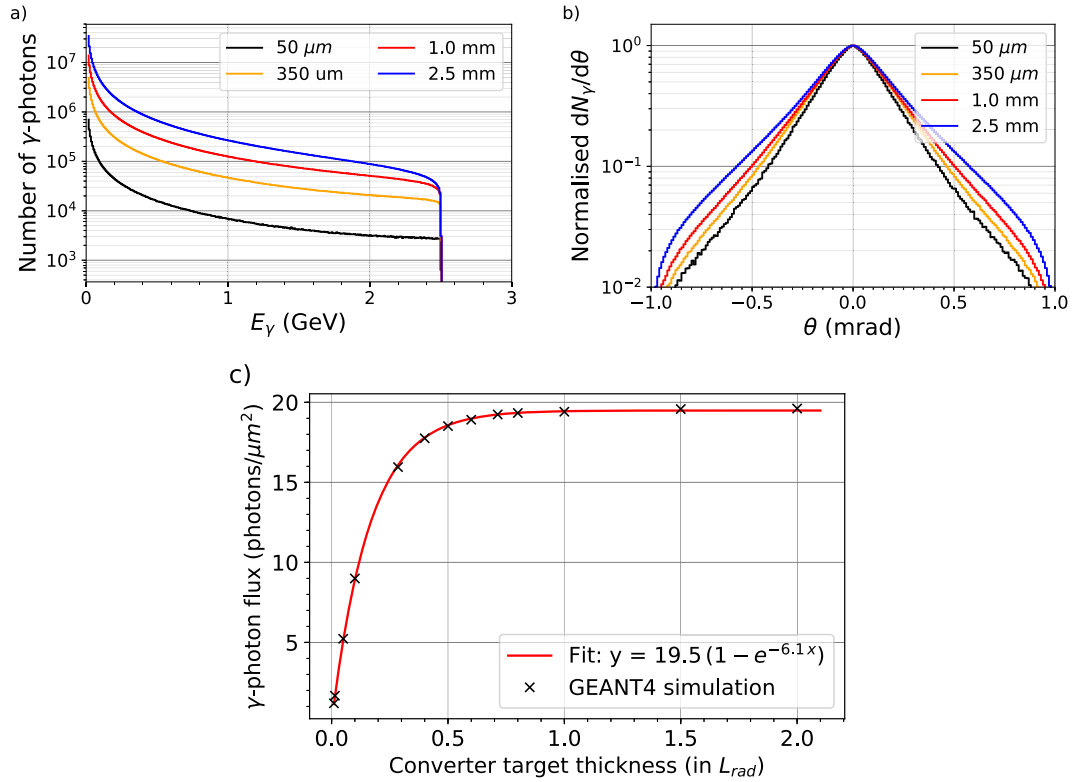
Figure 7. (a) Bremsstrahlung spectrum, (b) angular distribution of the Bremsstrahlung γ-ray for different tungsten converter target thickness (50 μm, 1.0 mm, 350 μm, 2.0 mm). As the thickness of the converter target increases, the overall number of γ-photons yield increases and relatively more photons are scattered to larger angles due to the multiple scattering inside the target. (c) γ-photon flux for different target thicknesses at the focal plane of the collider laser for energies 2.2 . . . 2.5 GeV in the central 100 μrad of the bremsstrahlung cone. As the target thickness increases, a saturation of the photon flux is observed for $L \ll L_{\mathrm{rad}}$. The simulations were performed using GEANT4 for a collimated electron beam with energy 2.5 GeV and a 10 pC charge.

power of 0.32 Tm which allows the charge and spectrum of the LWFA beam to be monitored. In addition, the electron beam dipole magnet ensures an interaction free of high energy electrons. In the limit of thin targets the divergence θ_{γ} of the γ-ray beam is determined by the Lorentz-factor $\gamma_{\mathrm{e}} \approx 5000$ of the electron beam $\theta_{\gamma} = 1/\gamma_{\mathrm{e}}$ or the divergence of the electron beam, whichever is the greater. For our design parameters the distance from the LWFA exit is $D = 600$ mm leading to an expected γ-beam spot size of $w_{\gamma} \approx 300$ μm assuming a divergence angle of the γ-ray beam given by $(\theta_{\mathrm{e}}^2 + \theta_{\gamma}^2)^{1/2} \approx 500$ mrad.

To match the beam intensity to the optimum a parabola with $f/2$ focussing was chosen, resulting in an Airy-focus with diameter of the first minimum at $q_1 = 2.44 \cdot f/\# \cdot \lambda \approx 4$ μm and Airy FWHM diameter of $\mathrm{FWHM}_{\mathrm{Airy}} = 1.03 \cdot f/\# \cdot \lambda \approx 1.65$ μm. Approximating the Airy-focus as a Gaussian we obtain an effective beam waist of $w_0 \approx 1.4$ μm and FWHM diameter of 1.6 μm. The relatively large γ-beam spot makes spatial overlap uncritical and will be achieved by overlapping the laser spot with the scintillation signal on a thin Ce:Yag scintillator. On the downside, the large γ-spot results in a small overlap fraction $(w_0/w_{\gamma})^2$ and reduces the possible pair yield significantly. As shown above, the pair yield also depends on the crossing angle θ, see figure 3(b), favouring head-on collision geometries and therefore arrangements where the focussing parabola is centred on the γ-beam axis. Such focussing arrangements, requiring a focussing parabola with a hole, were considered. For smaller values of θ the benefit of the slightly increased cross-section is outweighed by the intensity losses sustained for central holes that are large enough to produce negligible additional background. In our configuration the collision angle is set at 162°.

The splitting of the laser beam into LWFA and high-intensity beam after the laser chain is well suited to achieving high timing stability and this will be monitored interferometrically on a single shot basis. Since the electron bunches from LWFA are typically of the order of a few femtoseconds duration, the required timing accuracy $\Delta \tau$ is determined by the Rayleigh range of the high-intensity beam with $\Delta \tau < \pi w_0^2/(c \lambda) \approx 30$ fs—well within the expected stability of the system.
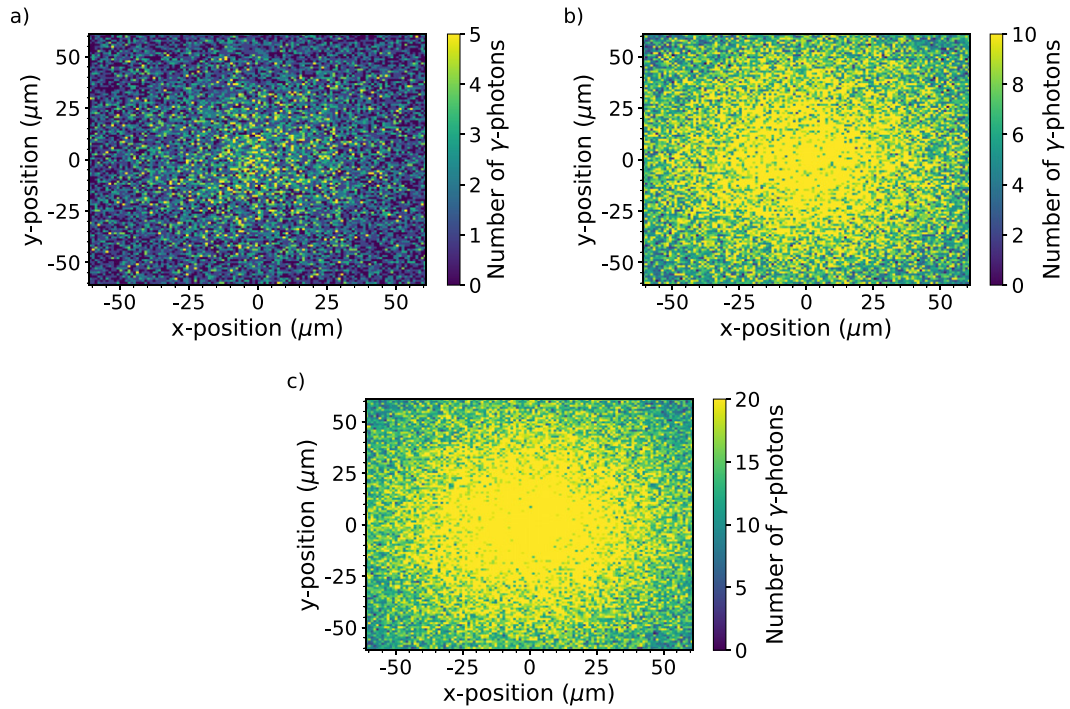
Figure 8. Simulated flux of the γ-ray beam in the spectral range of 2.2–2.5 GeV as a function of the tungsten target thickness: (a) 50 μm, (b) 350 μm, (c) 1000 μm, for a collimated electron beam with energy of 2.5 GeV and 10 pC of charge at the interaction laser focal plane. The increased yield for thicker targets is primarily radiated into larger angles and only increase peak flux slowly. The interaction laser only subtends an area of $\approx 2.0\ \mu m^2$—much smaller than γ-spot size. The peak flux of the gamma-beam in the considered spectral range is 1.7 photons μm^{-2}, 9.0 photons μm^{-2}, 16 photons μm^{-2}, respectively.

4. Pair production rate

We can now estimate the expected pair yield N_{pairs} for the experiment per primary electron bunch. In doing so we proceed by averaging the pair production probability per cycle P over the top 10% bremsstrahlung spectrum obtaining the pair yield per incident primary electron from the LWFA stage,

$$N_{\mathrm{pairs}} = \Phi_{\mathrm{gamma}} \cdot A_{\mathrm{laser}} \cdot \theta_{\mathrm{div}} \cdot N_{\mathrm{cycles}} \cdot P. \tag{7}$$
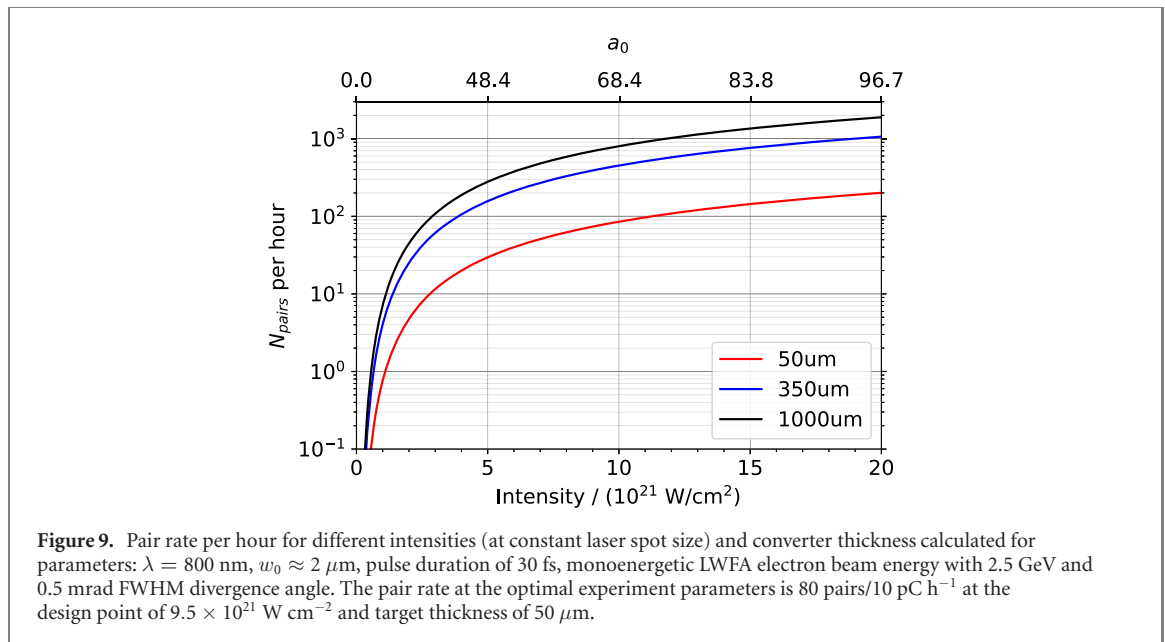
where Φ_{gamma} is the gamma-photon flux provided in figure 8 for different target thickness, A_{laser} is the collider laser focal spot area, N_{cycles} is the number of laser cycles and P is the average pair production probability per cycle as provided in figure 3(a). Note that the photon flux Φ_{γ} in figure 8 was calculated for collimated electron beam with zero source size.

The constant factor θ_{div} represents the 'divergence loss' of the bremsstrahlung flux, which in our setup is dominated by the divergence of the electron beam θ_e and, which is given by $\theta_{\mathrm{div}} = \theta_{\gamma}^2/(\theta_{\gamma}^2 + \theta_e^2) \approx 0.14$, where θ_{γ} is the divergence of the bremsstrahlung photons for collimated electrons.

While the pair conversion rate per γ photon is high, reaching over 50% at the centre of the laser focus, the overlap of the laser spot with the γ-beam is small therefore reducing the number of gamma-laser interactions.

Based on a charge of 10 pC per shot we find that our design point can achieve a maximum number of created positrons of 0.22 per laser shot. Figure 9 presents the pair yield expected per hour for different converter target thicknesses for 0.1 Hz repetition rate. Therefore, at our design point (electron energy of $E_0 = 2.5$ GeV with divergence $\theta_e = 0.5$ mrad, 50 μm tungsten converter foil and collider laser intensity of 9.5×10^{21} W cm^{-2}), the pair yield is expected to be of the order of 80 pairs per hour. Much higher pair production rates of > 1000 pairs/h are possible with thicker targets and higher bunch charges, which could realistically reach 100 pC per shot.

Note that the calculated pair yields are based on a constant laser spot-size and a γ-ray divergence of 0.5 mrad set by the LWFA beam. Adding a collimating lens after the LWFA stage would allow the divergence of a 2.5 GeV bremsstrahlung beam to be reduced to $\approx 1/\gamma = 0.2$ mrad and commensurately higher γ-ray flux and pair yield. Varying the laser intensity by maintaining constant laser pulse energy but increasing the laser spot-size results in a slower decay of the pair yield than the case considered in figure 9. The experimentally accessible intensity range is therefore greater than might be inferred from the figure and

Figure 9. Pair rate per hour for different intensities (at constant laser spot size) and converter thickness calculated for parameters: $\lambda = 800$ nm, $w_0 \approx 2$ μm, pulse duration of 30 fs, monoenergetic LWFA electron beam energy with 2.5 GeV and 0.5 mrad FWHM divergence angle. The pair rate at the optimal experiment parameters is 80 pairs/10 pC h^{-1} at the design point of 9.5×10^{21} W cm^{-2} and target thickness of 50 μm.

measurements in the range of $0.5 < \chi_\gamma < 2$ are feasible. The ability to vary the LWFA electron-beam energy will allow the impact of γ-ray energy on the cross-section to be evaluated experimentally in the range of $2 \ldots 5$ GeV.

5. Detection and backgrounds

The limitation of the design point to 50 μm thin targets and low charge beams may seem surprizing given the substantial reduction in pair yield by approximately two orders of magnitude and is explained by maintaining low backgrounds in a detector system with low granularity and tracking capability.

While single GeV leptons are easily detected with a variety of different approaches, the challenge is to ensure a sufficiently high SNR in the presence of 10^8 GeV electrons and a similar number of γ-ray photons with energies above 10 MeV. Care needs to be taken to prevent the production of high energy leptons via Bethe–Heitler pair production and Compton scattering.

The detector system consists of a multi-channel lead glass Cherenkov calorimeter with LYSO screens. Both systems have ns-scale temporal resolution to suppress scattering (e.g. from the beam dump) that arrives at the detectors with significant time delay. This system is described in detail in [46].

For the entire range of pair rates considered in figure 9 the BW leptons will be detected as single events (no pile-up) per detector resolution element in both LYSO and Cherenkov detectors. Therefore each BW-event results in well defined signal on the detectors that does not depend on the converter thickness L or the beam charge.

By contrast, the backgrounds scale linearly with beam charge and increase non-linearly when converter thickness is taken into account. This behaviour can be understood by considering the bremsstrahlung emission previously presented. In figure 7, we see that the overall yield of bremsstrahlung photons increases linearly with converter thickness for the range of L of interest here, while the spectral component > 2.2 GeV saturates for small values of $L < 0.5$. Additionally, we find that the ratio of peak γ-intensity to the wide-angle radiation decreases with converter length L as seen in figure 7(b). While the useful γ-conversion in the top 10% of the spectrum increases only by a factor of ≈ 2 the signal at close to 1 mrad increases 4 fold when the converter thickness reaches 2.5 mm. To optimise the SNR we therefore find thin converter foils with $L \ll L_{\rm rad}$ to be ideal with our design choosing 50 μm W-foil (compared to 3.5 mm radiation length).

We conducted GEANT4 [47–49] simulations as shown in figure 10 taking into account the full experimental geometry. For a 50 μm converter foil our simulations indicate only a small number of background events after temporal gating of the detectors as shown in figure 11 and therefore a signal to noise ratio (SNR) of > 10 for a 500 MeV lepton incident on the Cherenkov detectors. This reduces to SNR < 1 for the thicker target considered.
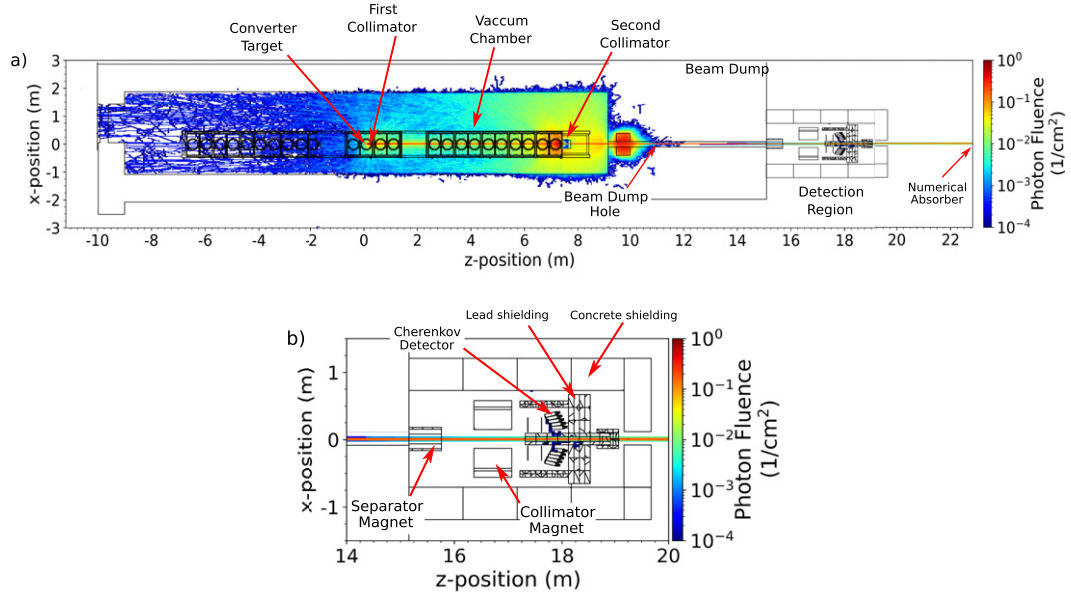
Figure 10. Simulated average γ-photon fluence at the target area and detector region at CALA. (a) Shows the photon flux across the entire target area as well in the detection region, and (b) presents a detailed view inside the detection region. The photon fluence is average over 10^4 primary events where each event corresponds to a shot of an collimated electron with energy of 2.5 GeV onto the tungsten converter target of 50 μm thickness. A numerical absorber is included in the simulations to represent the temporal gating of the detectors and all mitigate all backscattered noise from the beam dump.
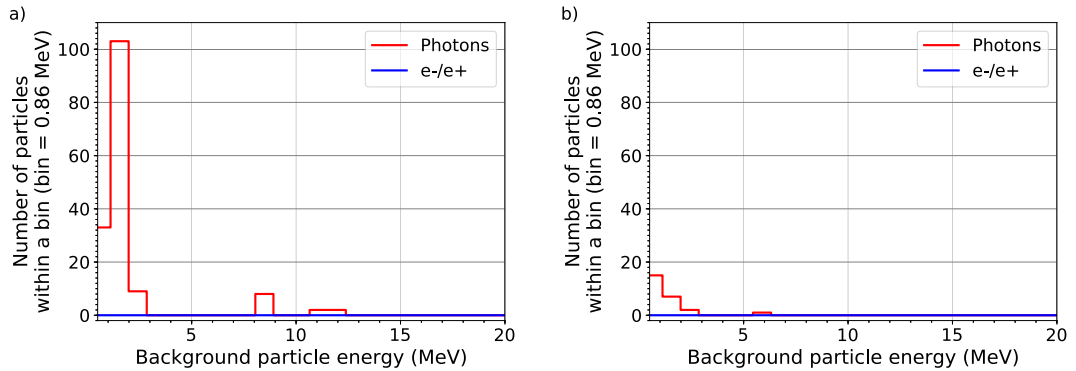

Figure 11. Simulated background noise at a single Cherenkov calorimeter channel (a) without employing temporal gating and (b) using temporal gating. By applying temporal gating on the detectors, the backscattered noise from the beam dump is mitigated and the noise on the detectors is only composed by the forward particle noise. Simulations were performed using GEANT4 with a collimated primary monoenergetic electron beam of 2.5 GeV and 10 pC of charge interacting with a 50 μm tungsten converter target.

6. Conclusion

In conclusion we have demonstrated a fully simulated design to measure the non-linear BW effect using an all-optical set-up. Ensuring a detectable and sufficiently high signal rate requires balancing a range of requirements within a large parameter space. An important consideration in optimising the experimental design is to maximise the SNR at detectable signal rates rather than maximising the signal rate itself. Counterintuitively, the trade-off between signal rate and SNR optimises for sufficiently thin bremsstrahlung converter foils at moderate charge ($L \ll L_{\mathrm{rad}}$) and an *e*-beam energy limited to 2.5 GeV—significantly below the achievable maximum. Similarly, rather than simply maximising the laser intensity, there is an *e*-beam energy dependent optimum in the mid-10^{21} W cm^{-2} range. Under these conditions experimentally viable yields are predicted with very low background. Introduction of a plasma-lens to focus the electron beam can increase the signal rates by up to a further order of magnitude.

Acknowledgments

Data availability statement

The data that support the findings of this study are available upon reasonable request from the authors.

ORCID iDs

F C Salgado ⬤ https://orcid.org/0000-0002-9109-9370
D Seipt ⬤ https://orcid.org/0000-0003-3695-0051

References

[1]   Breit G and Wheeler J A 1934 *Phys. Rev.* **46** 1087–91
[2]   Strickland D and Mourou G 1985 *Opt. Commun.* **56** 219–21
[3]   Lureau F *et al* 2020 *High Power Laser Sci. Eng.* **8** e43
[4]   Leemans W P, Nagler B, Gonsalves A J, Tóth C, Nakamura K, Geddes C G R, Esarey E, Schroeder C B and Hooker S M 2006 *Nat. Phys.* **2** 696–9
[5]   Pukhov A and Meyer-ter-Vehn J 2002 *Appl. Phys.* B **74** 355–61
[6]   Modena A *et al* 1995 *Nature* **377** 606–8
[7]   Keitel C H *et al* 2010 Photo-induced pair production and strong field QED on Gemini (arXiv:2103.06059v1)
[8]   Blackburn T G and Marklund M 2018 *Plasma Phys. Control. Fusion* **60** 054009
[9]   Hartin A, Ringwald A and Tapia N 2019 *Phys. Rev.* D **99** 036008
[10] Abramowicz H *et al* 2019 Letter of intent for the LUXE experiment (arXiv:1909.00860)
[11] Abramowicz H *et al* 2021 Conceptual design report for the LUXE experiment (arXiv:2102.02032)
[12] Meuren S 2019 Probing strong-field QED at FACET-II (SLAC E-320)
      https://conf.slac.stanford.edu/facet-2-2019/sites/facet-2-2019.conf.slac.stanford.edu/files/basic-page-docs/sfqed_2019.pdf
[13] Schwinger J 1951 *Phys. Rev.* **82** 664–79
[14] Sauter F 1931 *Z. Phys.* **69** 742–64
[15] Reiss H R 1962 *J. Math. Phys.* **3** 59–67
[16] Reiss H R 1971 *Phys. Rev. Lett.* **26** 1072–5
[17] Dunne G V 2009 *Eur. Phys. J.* D **55** 327–40
[18] Nikishov A I 1985 *J. Russ. Laser Res.* **6** 619–717
[19] Ritus V I 1985 *J. Russ. Laser Res.* **6** 497–617
[20] Nikishov A I and Ritus V I 1964 *Sov. Phys. J. Exp. Theor. Phys.* **19** 529
[21] Bula C *et al* 1996 *Phys. Rev. Lett.* **76** 3116–9
[22] Burke D L *et al* 1997 *Phys. Rev. Lett.* **79** 1626–9
[23] Bamber C *et al* 1999 *Phys. Rev.* D **60** 092004
[24] Research Unit FOR 2783 2021 Probing the quantum vacuum http://quantumvacuum.org (accessed 30 June 2021)
[25] Samarin G M, Zepf M and Sarri G 2018 *J. Mod. Opt.* **65** 1362–9
[26] Tajima T and Dawson J M 1979 *Phys. Rev. Lett.* **43** 267–70
[27] Esarey E, Schroeder C B and Leemans W P 2009 *Rev. Mod. Phys.* **81** 1229–85
[28] Kettle B *et al* 2021 A laser-plasma platform for photon-photon physics (arXiv:2106.15170)
[29] Poder K *et al* 2018 *Phys. Rev.* X **8** 031004
[30] Corvan D J, Dzelzainis T, Hyland C, Nersisyan G, Yeung M, Zepf M and Sarri G 2016 *Opt. Express* **24** 3127–36
[31] Erber T 1966 *Rev. Mod. Phys.* **38** 626–59
[32] Nousch T, Seipt D, Kämpfer B and Titov A I 2012 *Phys. Lett.* B **715** 246–50
[33] Krajewska K and Kamiński J Z 2012 *Phys. Rev.* A **86** 052104
[34] Pike O J, Mackenroth F, Hill E G and Rose S J 2014 *Nat. Photon.* **8** 434–6
[35] Meuren S, Keitel C H and Di Piazza A 2016 *Phys. Rev.* D **93** 085028
[36] Di Piazza A 2016 *Phys. Rev. Lett.* **117** 213201
[37] Jansen M J A and Müller C 2017 *Phys. Lett.* B **766** 71–6
[38] Blackburn T G, Ilderton A, Murphy C D and Marklund M 2017 *Phys. Rev.* A **96** 022128
[39] Titov A I, Takabe H and Kämpfer B 2018 *Phys. Rev.* D **98** 036022
[40] Zhang P, Bulanov S S, Seipt D, Arefiev A V and Thomas A G R 2020 *Phys. Plasmas* **27** 050601
[41] Golub A, Villalba-Chávez S, Ruhl H and Müller C 2021 *Phys. Rev.* D **103** 016009
[42] Gonsalves A J *et al* 2019 *Phys. Rev. Lett.* **122** 084801
[43] Lu W, Tzoufras M, Joshi C, Tsung F S, Mori W B, Vieira J, Fonseca R A and Silva L O 2007 *Phys. Rev. Spec. Top. Accel. Beams* **10** 061301
[44] Dromey B, Kar S, Zepf M and Foster P 2004 *Rev. Sci. Instrum.* **75** 645–9
[45] Group P D *et al* 2020 *Prog. Theor. Exp. Phys.* 083C01
[46] Salgado F C *et al* 2021 Single particle detection system for strong-field QED experiments (arXiv:2107.03697)
[47] Agostinelli S *et al* 2003 *Nucl. Instrum. Methods* A **506** 250–303
[48] Allison J *et al* 2016 *Nucl. Instrum. Methods* A **835** 186–225
[49] Allison J *et al* 2006 *IEEE Trans. Nucl. Sci.* **53** 270–8